AGU PUBLICATIONS

JGR

Journal of Geophysical Research: Biogeosciences

RESEARCH ARTICLE
10.1002/2015JG003150

Key Points:
- The GOME-2 SIF reveals contrasting onset mechanisms of two major droughts in U.S. Great Plains
- Reduction of SIF during drought was caused by both decreased fPAR and fluorescence yield
- Anomalies of SIF and root zone soil moisture are significantly correlated in the study area

Supporting Information:
- Supporting Information S1

Correspondence to:
Y. Sun,
suny@jsg.utexas.edu

Citation:
Sun, Y., R. Fu, R. Dickinson, J. Joiner, C. Frankenberg, L. Gu, Y. Xia, and N. Fernando (2015), Drought onset mechanisms revealed by satellite solar-induced chlorophyll fluorescence: Insights from two contrasting extreme events, *J. Geophys. Res. Biogeosci.*, *120*, 2427–2440, doi:10.1002/2015JG003150.

Received 11 JUL 2015
Accepted 27 OCT 2015
Accepted article online 2 NOV 2015
Published online 25 NOV 2015

Drought onset mechanisms revealed by satellite solar-induced chlorophyll fluorescence: Insights from two contrasting extreme events

Ying Sun[1], Rong Fu[1], Robert Dickinson[1], Joanna Joiner[2], Christian Frankenberg[3], Lianhong Gu[4], Youlong Xia[5], and Nelun Fernando[6]

[1]Department of Geological Sciences, Jackson School of Geosciences, University of Texas at Austin, Austin, Texas, USA, [2]NASA Goddard Space Flight Center, Greenbelt, Maryland, USA, [3]Jet Propulsion Laboratory, California Institute of Technology, Pasadena, California, USA, [4]Environmental Science Division and Climate Change Science Institute, Oak Ridge National Laboratory, Oak Ridge, Tennessee, USA, [5]I. M. Systems Group, Environmental Modeling Center, National Centers for Environmental Prediction, College Park, Maryland, USA, [6]Texas Water Development Board, Austin, Texas, USA

Abstract This study uses the droughts of 2011 in Texas and 2012 over the central Great Plains as case studies to explore the potential of satellite-observed solar-induced chlorophyll fluorescence (SIF) for monitoring drought dynamics. We find that the spatial patterns of negative SIF anomalies from the Global Ozone Monitoring Experiment 2 (GOME-2) closely resembled drought intensity maps from the U.S. Drought Monitor for both events. The drought-induced suppression of SIF occurred throughout 2011 but was exacerbated in summer in the Texas drought. This event was characterized by a persistent depletion of root zone soil moisture caused by yearlong below-normal precipitation. In contrast, for the central Great Plains drought, warmer temperatures and relatively normal precipitation boosted SIF in the spring of 2012; however, a sudden drop in precipitation coupled with unusually high temperatures rapidly depleted soil moisture through evapotranspiration, leading to a rapid onset of drought in early summer. Accordingly, SIF reversed from above to below normal. For both regions, the GOME-2 SIF anomalies were significantly correlated with those of root zone soil moisture, indicating that the former can potentially be used as proxy of the latter for monitoring agricultural droughts with different onset mechanisms. Further analyses indicate that the contrasting dynamics of SIF during these two extreme events were caused by changes in both fraction of absorbed photosynthetically active radiation fPAR and fluorescence yield, suggesting that satellite SIF is sensitive to both structural and physiological/biochemical variations of vegetation. We conclude that the emerging satellite SIF has excellent potential for dynamic drought monitoring.

1. Introduction

Drought is among the most damaging and least understood climate extremes in many regions of the world. In the U.S. alone, drought has led to losses of hundreds of billions of dollars during the last three decades [*Smith and Matthews*, 2015]. The U.S. Great Plains is particularly vulnerable to drought, as evident by the extreme events in the 1930s ("Dust Bowl") and 1950s [*Cook et al.*, 2007], as well as the 2011 Texas drought [*Seager et al.*, 2014] and the 2012 drought in the central Great Plains [*Hoerling et al.*, 2014]. Further, an increasing drought risk that accompanies the warming trend in the 21st century is projected in this region by state-of-the-art general circulation models [*Cook et al.*, 2015], although the severity is uncertain [e.g., *Hoerling et al.*, 2012]. As a major "bread basket," the Great Plains' high vulnerability to drought threatens both regional and global food security.

There is an urgent need for a system of early warning and real-time monitoring of emerging drought that can provide information on plant physiological stress for agricultural planning and mitigation in this region. Such a system can benefit from existing drought-monitoring efforts, such as the North American Land Data Assimilation System (NLDAS) Drought Monitor [*Sheffield et al.*, 2012; *Xia et al.*, 2014a] and the U.S. Drought Monitor (USDM) [*Svoboda et al.*, 2002]. In particular, the latter uses various indicators to track different components of the water cycle, e.g., precipitation, soil moisture, streamflow, and runoff, providing both quantitative (drought intensities) and qualitative (assessment of social impacts) information on water status at varying time scales.

Satellite observations of vegetation status, which is strongly influenced by soil water stress, complement ground- and model-based operational systems such as those of the USDM and NLDAS. The routine availability of normalized difference vegetation index (NDVI) data sets has led to the development of operational drought monitoring systems based on vegetation status information. For example, the VegDRI system uses the vegetation drought response index, which integrates NDVI-derived vegetation anomalies and climate-related variables as well as biophysical parameters of soils and land cover/use, for real-time drought monitoring across the contiguous U.S. [*Brown et al*., 2008; *Wardlow et al*., 2012]. The DroughtView system, hosted by the University of Arizona (http://droughtview.arizona.edu/), also relies on high-resolution NDVI products to monitor drought in the southwestern U.S. Various extended indices built upon NDVI have been developed to improve the characterization of drought, for example, the vegetation condition index [*Liu and Kogan*, 1996], vegetation health index [*Kogan*, 1995], and drought severity index [*Mu et al*., 2013]. The enhanced vegetation index [*Huete et al*., 2002], developed to overcome some shortcomings of the NDVI (e.g., atmospheric contamination and saturation with dense canopies), has also been widely applied to characterize drought, for example, the forest response to drought in the Amazon [*Xu et al*., 2011] and in Congo [*Zhou et al*., 2014].

While hydrology- and vegetation-index-based methods are indispensable for monitoring large-scale drought events, the information they provide is only indirectly related to vegetation functioning. From the perspective of agricultural planning and mitigation, stress-induced degradation in vegetation functioning is a more direct indicator of increased risk of reduction in plant productivity and crop failure. In this regard, detecting and monitoring drought dynamics based on the newly available satellite retrievals of solar-induced chlorophyll fluorescence (SIF) offer the potential to complement existing methods and provide critical information that meets planning and mitigation needs in agriculturally important regions such as the U.S. Great Plains.

The SIF is essentially a "glow" of plants under sunlight. The absorbed photosynthetically active radiation (APAR) by a leaf has several potential fates. In addition to being used to drive photochemical reactions to reduce atmospheric CO_2 (photosynthesis), it can be reemitted as fluorescence at longer wavelengths. The absorbed energy can also undergo radiationless decay or be lost through regulated nonphotochemical quenching (NPQ) processes [*Baker*, 2008]. As a consequence of energy conservation, variations in SIF contain information about plant biochemical, physiological, and metabolic functions as well as the amount of APAR. If drought induces changes in these functions, such changes will necessarily result in changes in SIF, usually reductions of both the photosynthesis and fluorescence yield [*Flexas et al*., 2002; *Daumard et al*., 2010]. Indeed, *Damm et al*. [2015] used airborne sensors to show that there is an ecosystem-specific relationship between gross photosynthesis and far-red SIF. Therefore, both on theoretical and empirical grounds, satellite SIF has been considered to be the most directly measurable signal of terrestrial photosynthesis from space [*Frankenberg et al*., 2011b].

Although, so far, no satellite has been specifically designed and launched for SIF measurements, the potential of such information has motivated a number of researchers to derive SIF signals from spectral measurements obtained by existing satellite platforms [*Guanter et al*., 2007, 2012; *Frankenberg et al*., 2011b; *Joiner et al*., 2011, 2012, 2013]. These satellite SIF signals have been shown to be highly correlated with terrestrial gross primary production for natural vegetation [*Frankenberg et al*., 2011b] and croplands [*Guanter et al*., 2014] and with the seasonality of carbon uptake at flux tower sites [*Joiner et al*., 2014]. These studies suggest that SIF is an important, perhaps also the most direct, remotely sensed measure of vegetation canopy functioning.

Fluorescence has been used to study water stress at different spatial scales. *Flexas et al*. [2002] found a decrease of fluorescence yield under water stress for C3 leaves. *Daumard et al*. [2010] reported a reduction of canopy-scale fluorescence during a drought episode even though canopy greenness remained unchanged. This finding suggested that SIF may have a higher sensitivity to vegetation stress than vegetation indices that measure only plant greenness. *Lee et al*. [2013] quantified the degree of drought stress on productivity of the Amazon rainforest by using SIF measured by the Japanese Greenhouse-gases Observing SATellite (GOSAT).

To ascertain the potential of using satellite SIF to detect and monitor drought development in the context of agricultural planning and mitigation, it is essential to examine the role of soil moisture, particularly that of root zone water content, in the SIF-drought relationship. Drought causes soil moisture deficit, which in turn leads to stomatal closure and reduction in photosynthesis and transpiration, important plant functions that

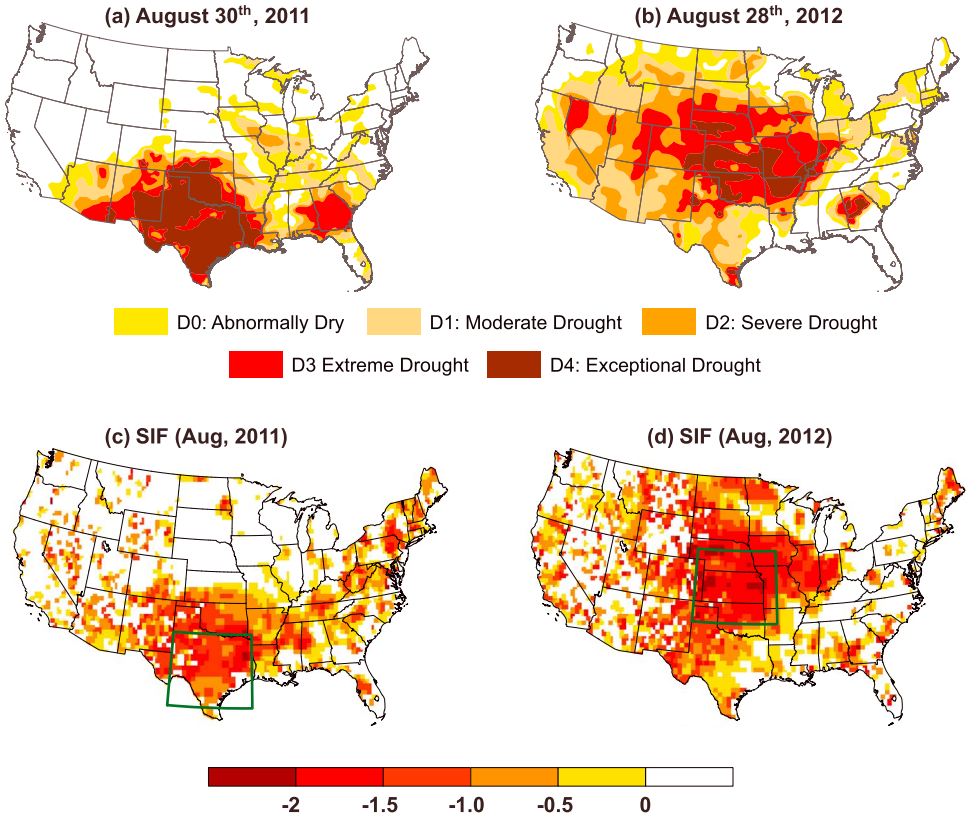

Figure 1. Drought intensity and its impact on vegetation of the two extreme drought events: (a, c) the 2011 Texas drought and (b, d) the 2012 drought in the central Great Plains. Figures 1a and 1b show the spatial extent of the drought category in the last week of August, i.e., 30 August 2011 (for the Texas drought) and 28 August 2012 (for the central Great Plains drought). Data are from the U.S. Drought Monitor. Figures 1c and 1d show the anomalies of the solar-induced chlorophyll fluorescence (SIF) in August. Here the anomalies are normalized by the standard deviation in order to make the SIF signals spatially comparable. The green boxes (27–34°N, 94–103°W for Texas, and 35–42°N, 93–103°W for the central Great Plains, respectively) highlight the regions that are used for deriving the region-wide averages.

affect fluorescence yield [*Baker*, 2008]. Severe droughts may result in acute shortage of soil moisture across the whole rooting depth of plants, causing leaf wilting and loss of chlorophyll [*Hsiao*, 1973]. The consequence of these effects may be reduction in the capacity of vegetation to absorb PAR and therefore a suppression in SIF. Consequently, the change of SIF is expected to be closely related to that of soil moisture integrated across the root zone but their phase relationship may depend on the intensity of soil moisture deficit.

We test this hypothesized linkage by investigating two contrasting extreme drought events in the U.S. Great Plains: the 2011 Texas drought and the 2012 drought in the central Great Plains (Figure 1 and Figure S1 in the supporting information). In 2011, Texas endured the most extreme single-year drought since 1895, with nearly the entire state area falling under the USDM "Exceptional Drought" category (the highest intensity D4) in the summertime of the year (Figure 1a). The annual rainfall fell to only 40% of its long-term mean, resulting in severe soil moisture deficits [*Long et al.*, 2013]. This drought caused $7.6 billion in agricultural losses [*Fannin*, 2012]. The associated unprecedented high temperatures induced numerous wildfires that burned almost 4 million acres across Texas [*Combs*, 2012].

In the summer of 2012, over three quarters of the contiguous U.S. experienced unusually dry conditions; in particular, states in the central Great Plains suffered extreme drought (Figure 1b). With rainfall only at half of the long-term mean, this event was the most severe seasonal drought in the central Great Plains in more than a century [*Hoerling et al.*, 2014]. Economic losses were over $30 billion as estimated by the National Climatic Data Center (http://www.ncdc.noaa.gov/billions/events), and substantial decreases in maize and soybean production were reported by the U.S. Department of Agriculture [*Gilbert*, 2012].

These two drought events represent an opportunity for a comparative study of the drought-soil moisture-SIF relationships because they differed in the development of the drought dynamics and occurred in regions with contrasting water management practices. The Texas drought was characterized by persistent deficits in precipitation that started from late 2010 [*Seager et al*., 2014], and the induced soil moisture depletion intensified throughout spring and summer in 2011 [*Long et al*., 2013]. In contrast, the 2012 drought in the central Great Plains was preceded by relatively normal precipitation and warmer surface temperature in spring followed by an abrupt rainfall reduction and abnormally high temperatures in summer, typifying a "flash" drought [*Hoerling et al*., 2014; *Mo and Letternmaier*, 2015]. The two drought extremes happened within the era of the satellite SIF observations, making them ideal examples to study the response of SIF to drought.

In this study, we aim to address the following questions: (1) Can SIF detect the differences in the temporal progression and spatial extension of the two contrasting droughts? (2) How are the temporal and spatial dynamics of SIF related to those of soil moisture, precipitation, temperature, and evapotranspiration (ET) under these two different drought regimes? (3) How do different processes contribute to drought-induced changes in SIF (i.e., changes in APAR versus fluorescence yield)? (4) What improvements are needed in the still relatively new satellite SIF measurements in order to better serve the needs of the large-scale agricultural community in terms of drought planning and mitigation?

2. Data and Methods

2.1. Framework for Interpreting Dynamics of SIF

Analogous to fluorescence emission from a leaf, SIF from a canopy (F) can be expressed as

$$F = \phi \times \mathrm{fPAR} \times \mathrm{PAR} = \phi \times \mathrm{APAR} \tag{1}$$

where fPAR is the fraction of absorbed PAR, i.e., APAR = fPAR × PAR and ϕ is defined as the effective fluorescence yield of the canopy; here ϕ can be considered as the product of the actual fluorescence yield of the canopy and the fraction of the canopy emission that escapes to the atmosphere. These two factors cannot be separated in satellite-based measurements; only their product ϕ can be determined, i.e., $\phi = F/(\mathrm{fPAR} \times \mathrm{PAR}) = F/\mathrm{APAR}$, where F, fPAR, and PAR can be estimated from remotely sensed variables. For examination of the relative changes under clear-sky conditions, as is done in this study, the absolute value of PAR is not needed. Instead, one could simply examine spatial and temporal variations in

$$\frac{F}{\cos(Z)} \propto \phi \times \mathrm{fPAR}, \tag{2}$$

$$\frac{F}{\cos(Z) \times \mathrm{fPAR}} \propto \phi, \tag{3}$$

where cos(Z) is used as a proxy of PAR and Z is the solar zenith angle. Equation (2) describes the combined net effect on F resulting from changes in vegetation physiological and biochemical states, which primarily affect ϕ and in vegetation structural variables (e.g., chlorophyll content, LAI), which affect fPAR. Equation (3) isolates the effect on ϕ. *Yoshida et al*. [2015] used a similar approach for separating ϕ. Similar to light use efficiency models of photosynthesis widely used by the remote sensing community, equations (1)–(3) greatly simplify fluorescence emission, transfer, and absorption in a plant canopy by treating it as a big leaf. While such simplification ignores the complexities caused by the 3-D structure of a canopy, *Damm et al*. [2015] suggested with simulations of the Soil-Canopy Observations of Photosynthesis and Energy Balance model (SCOPE) [*van der Tol et al*., 2009] that the generally linear feature of these equations is adequate for separating changes in F caused by variations in fluorescence yield from that of APAR. Note also that equations (1)–(3) do not explicitly capture effects such as the impact of diffuse versus direct beam radiation on canopy fluorescence [*Yang et al*., 2015]. Since the present study focuses on clear-sky or nearly clear-sky conditions, the impact of variations in F caused by changing diffuse to direct beam ratios is minimized.

2.2. Satellite-Based SIF Data

Our study uses two satellite-based SIF data sets retrieved from different instruments. The first SIF product is inferred from the Global Ozone Monitoring Instrument 2 (GOME-2) on board Eumetsat's MetOp-A satellite. It

provides retrieval of the far-red chlorophyll fluorescence peaking at 740 nm, which is estimated from measurement over a broad spectral range (734–758 nm) [*Joiner et al*., 2013, 2014]. The retrieval employs a simplified radiative transfer model together with a principal component analysis to disentangle the spectral signatures of atmospheric absorption, surface reflectance, and fluorescence emission. The version 26 level 3 data set used here provides monthly global coverage of SIF observations at 0.5° × 0.5° spatial resolution and covers the period from 2007 to present.

In addition, we use SIF retrievals from the GOSAT [*Frankenberg et al*., 2011a, 2011b]. These retrievals are solely based on the in-filling of the Fraunhofer lines between 755 and 775 nm from spectra recorded by the Thermal And Near infrared Sensor for carbon Observation (TANSO) Fourier Transform Spectrometer (FTS). The TANSO-FTS high spectral resolution ensures a more robust and accurate SIF retrieval as atmospheric absorption, scattering, and albedo effects can be minimized using narrow spectral fitting windows [*Frankenberg et al*., 2011b]. However, the GOSAT SIF retrievals have a lower spatial resolution (4° × 4°) and shorter duration (2009–2012) as compared with GOME-2. We therefore primarily use the GOME-2 data set in our analyses. We further apply a local 3 × 3 window (1.5° × 1.5°) smoothing to minimize the noise inherent in the original retrieval.

2.3. Satellite-Based fPAR

We use the MODerate resolution Imaging Spectroradiometer (MODIS, Collection 5) MOD15A2 fPAR data set [*Myneni et al*., 2002] in our analyses. The fPAR data set is an 8 day composite at 1 km × 1 km. Its information to derive fPAR comes from the same reflectance used to compute vegetation indices such as NDVI. The primary purpose of using fPAR here is to identify its relative contribution to drought-induced decrease of SIF.

2.4. Soil Water Content Simulated by Land Surface Models

Ground measurements of root zone soil moisture are spatially sparse in the study regions, and remotely sensed soil moisture through microwave is generally restricted to the top few centimeters of soil. We therefore use the soil water content (SWC) simulated by the NLDAS Phase 2 (NLDAS-2) land surface models [*Xia et al*., 2012]. A major mission of NLDAS-2 is to provide support for the National Integrated Drought Information System. These NLDAS-2 models are driven by reanalysis of atmospheric forcing and run at 1/8° over the contiguous U.S. from 1979 to present. Here three-model products are used: the Mosaic [e.g., *Koster and Suarez*, 1992], Noah [e.g., *Ek et al*., 2003], and the Variable Infiltration Capacity (VIC) [e.g., *Liang et al*., 1994]. Mosaic has three soil layers: 0–10, 10–40, and 40–200 cm, and the centers of each layer are 5, 25, and 120 cm, respectively. Noah provides soil moisture at four soil depths with spatially fixed thicknesses, 0–10, 10–40, 40–100, and 100–200 cm centered at 5, 25, 70, and 150 cm, respectively. VIC has three soil layers; its first soil layer has a fixed thickness of 10 cm and the other two soil layers have depths spatially varying from grid to grid. These simulated soil moisture products have been evaluated with in situ measurements across the contiguous U.S. They generally capture the wet/dry events and have high correlation with measurements in terms of temporal variability although large biases exist in terms of absolute magnitude [*Xia et al*., 2014b]. Previous studies demonstrated the capability of NLDAS-2 Mosaic and Noah models to depict the depletion of soil water in the 2011 Texas drought [*Long et al*., 2013].

Here we use the SWC within the top 100 cm soil layer to represent the root zone soil moisture, as typically used for monitoring agricultural drought. For the VIC model, which has spatially varying soil layers, a vertical interpolation is performed to convert SWC into four uniform soil layers corresponding to those of the Noah model, following the protocol of *Xia et al*. [2014b]. We then compute the ensemble mean of root zone SWC from the three NLDAS-2 models and only use this ensemble mean in our analyses. This practice takes advantage of the fact that model simulation skills vary among regions and models, but their ensemble means generally show better performance than any individual model [*Xia et al*., 2014b]. The Noah model itself uses 100 cm root depth for grasslands and crops and 200 cm for woodland and forest, whereas the Mosaic model sets root depth to 40 cm for all vegetation types. The root depths of the VIC model vary from 135 cm to 300 cm, depending on vegetation type. Consequently, the use of the top 100 cm to calculate the mean SWC of the three models represents a compromise among the three models and appears to be characteristic of the root zone depth in the Great Plains.

2.5. Other Climate Variables

Multiple climate-related variables are employed to help interpret the temporal and spatial dynamics of SIF during the two drought events. They include precipitation, temperature at 2 m height from ground, and ET.

The 2 m temperatures and precipitation are from the NLDAS-2 climate forcing, derived from the NCEP North American Regional Reanalysis (NARR) [*Mesinger et al*., 2006] and NOAA Climate Prediction Center (CPC) gauge-based analyses, respectively. The three NLDAS-2 models share identical meteorological forcings. ET data are obtained from the NLDAS-2 model output, which have been shown to exhibit close correlation with MODIS and GRACE-based ET products in the southern Great Plains [*Long et al*., 2014] and have been comprehensively evaluated against flux tower observations [*Xia et al*., 2015]. We derive a three-model ensemble mean of ET as we do for the soil moisture.

2.6. Calculation of Anomalies

We calculate monthly anomalies of all the aforementioned variables to obtain drought stress-related signals. The anomalies are computed as a departure from their corresponding multiyear mean for each month. The multiyear mean and anomalies are established from 2007 to 2013 for all data sets. The GOSAT SIF data are only available from 2009 to 2012; thus its anomaly is calculated as departure from the average of this 4 year period.

2.7. Matching Spatial Resolution for Different Datasets

The spatial resolution of different data sets used in this study varies substantially. For example, the GOME-2 SIF has a spatial resolution of 0.5° while fPAR is at 1 km and the modeled SWC at 0.125°. Therefore, it is necessary to reprocess the data in order to minimize potential discrepancies resulting from the mismatch in spatial resolution for quantifying the relationships among SIF, root zone SWC, ET, and temperature. We spatially aggregate the finer resolution products, i.e., fPAR and SWC, to match the SIF grid size. In addition, the 8 day fPAR data set is temporally aggregated into monthly means, consistent with the SIF data set.

3. Results

Our analyses show that strong negative anomalies of GOME-2 SIF existed during the 2011 Texas drought and the 2012 central Great Plains drought and that their spatial patterns were consistent with the USDM mapping of these two events (Figures 1a and 1b). At the peak of the 2011 Texas drought (August), there were substantial SIF negative anomalies throughout Texas, with departures generally exceeding 1 standard deviation from the multiyear mean (Figure 1c). Large negative SIF anomalies were also observed in Oklahoma, southern Kansas, and western New Mexico. The areas with the largest negative SIF anomalies generally corresponded to those designated as exceptional drought (D4) by the USDM (Figure 1a). The GOSAT SIF anomalies exhibited a spatial pattern consistent with that of GOME-2 but with somewhat different amplitudes (Figure S2a). The latter difference is likely a combined consequence of the coarse resolution of the GOSAT data set, obscuring small-scale details, its inference of SIF at a different reference wavelength compared to GOME-2, and the different satellite overpass times.

The 2012 central Great Plains drought, which also peaked in August (Figure 1b), had a widespread reduction of SIF across Nebraska, Kansas, Iowa, Missouri, Illinois, Indiana, and Oklahoma (Figure 1d). Northwestern Texas, in contrast to the eastern Texas, also displayed a considerable negative SIF anomaly. The GOSAT SIF likewise captured this large-scale drought pattern across the central Great Plains and the spatial drought gradient in Texas (Figure S2b) but showed a much larger area with negative anomalies including the western Great Plains and eastern U.S., where the USDM indicated that drought was not as severe as in the central Great Plains (Figure 1b). Thus, our analyses demonstrate that satellite SIF available from current instruments has the potential to delineate the spatial extent of regions under the impact of drought, even though these instruments were not specifically designed for measuring SIF.

Can SIF also capture the dynamic process of drought development? For most months during the Texas drought in 2011, the spatially averaged GOME-2 SIF (averaged over 27–34°N, 94–103°W as highlighted in Figure 1c) was significantly smaller than the corresponding multiyear mean (Figure 2a). Here significance is considered as a departure >1 standard deviation. The difference between 2011 and the multiyear mean values was relatively small in spring but grew larger until near the end of 2011 when the drought was interrupted by precipitation (Figure 2e). The simulated ET showed a broadly similar temporal pattern, although subtle differences existed (Figure 2c). Presumably, the broad similarity between SIF and ET reflects the tight coupling between photosynthesis and transpiration [e.g., *Ball et al*., 1987]. These persistent negative vegetation responses were a consequence of the long-lasting soil water depletion in the root zone (Figure 2d)

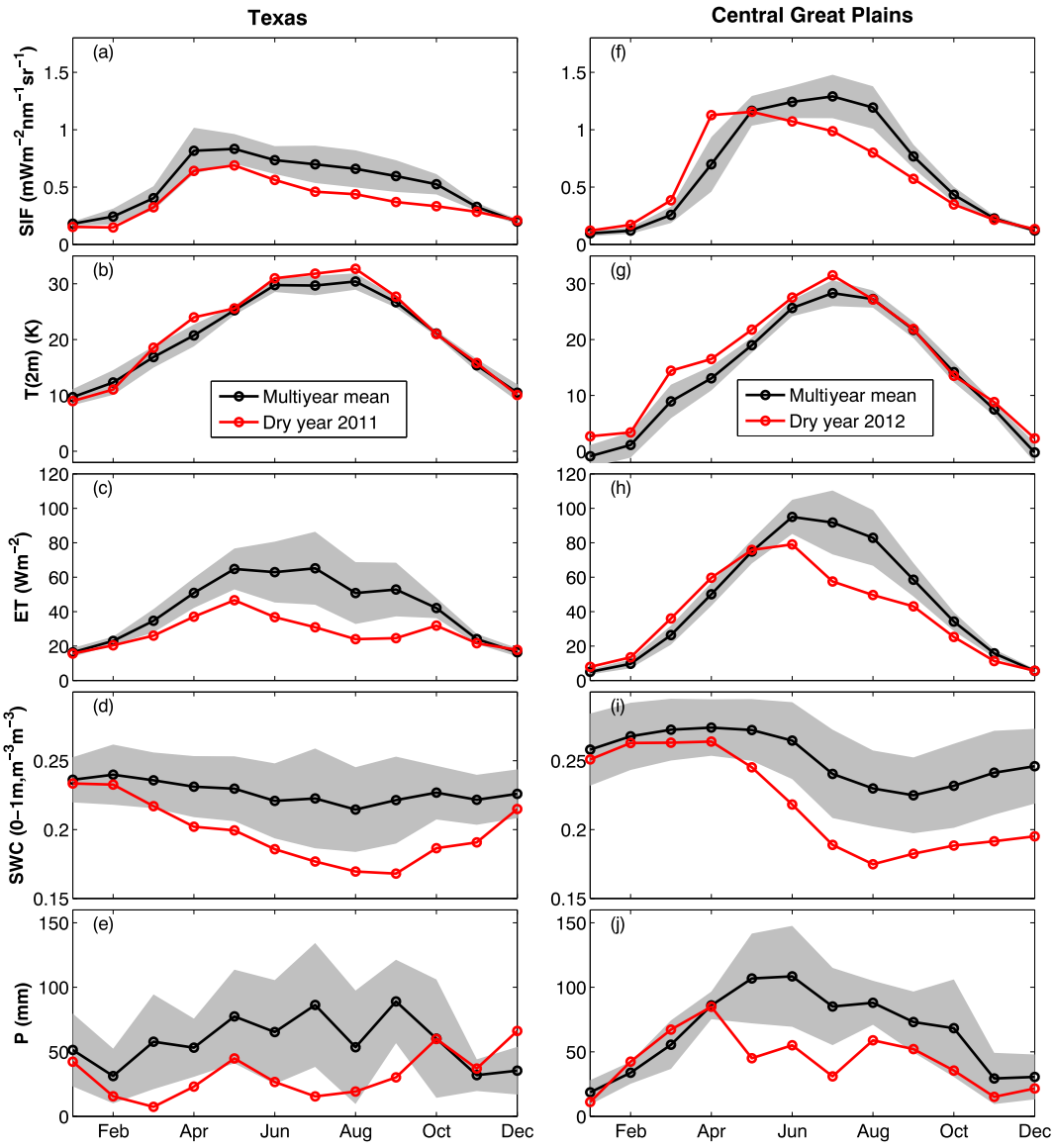

Figure 2. (a and f) The region-wide mean seasonal cycle of GOME-2 SIF, (b and g) temperature 2 m above ground (T2m), (c and h) evapotranspiration (ET), (d and i) soil water content (SWC) integrated through the plant root zone (0–1 m), and (e and j) precipitation (P) for Texas (left column) and for the central Great Plains (right column). The black curves represent the monthly multiyear mean of each variable between 2007 and 2013; the red curves show the seasonal evolution during the drought year (2011 for Texas and 2012 for the central Great Plains, respectively). The grey shaded area is the ±1 standard deviation of the multiyear mean.

caused by the large precipitation deficit throughout 2011 (Figure 2e), probably also exacerbated by anomalously high temperatures (Figure 2b). The soil water deficit maximized during summertime, corresponding to the maximum monthly depression in SIF. As the soil moisture started to recover near the end of 2011 following rainfall episodes, the SIF signal moved toward its multiyear mean (Figure 2a). However, although precipitation and soil moisture increased from a late summer minimum, SIF did not, probably because by that time vegetation had entered into a less active stage and seasonal PAR had peaked, as indicated by a general decline in the multiyear mean SIF (Figure 2a). The temporal dynamics of SIF and associated variables were also reflected in the spatial distributions of their anomalies for the spring and summer of 2011 in Texas (Figures 3a–3h).

The 2012 central Great Plains drought (35–42°N, 93–103°W as highlighted in Figure 1d) showed a different temporal pattern of drought development (Figures 2f–2j). In spring 2012, the monthly GOME-2 SIF rose more

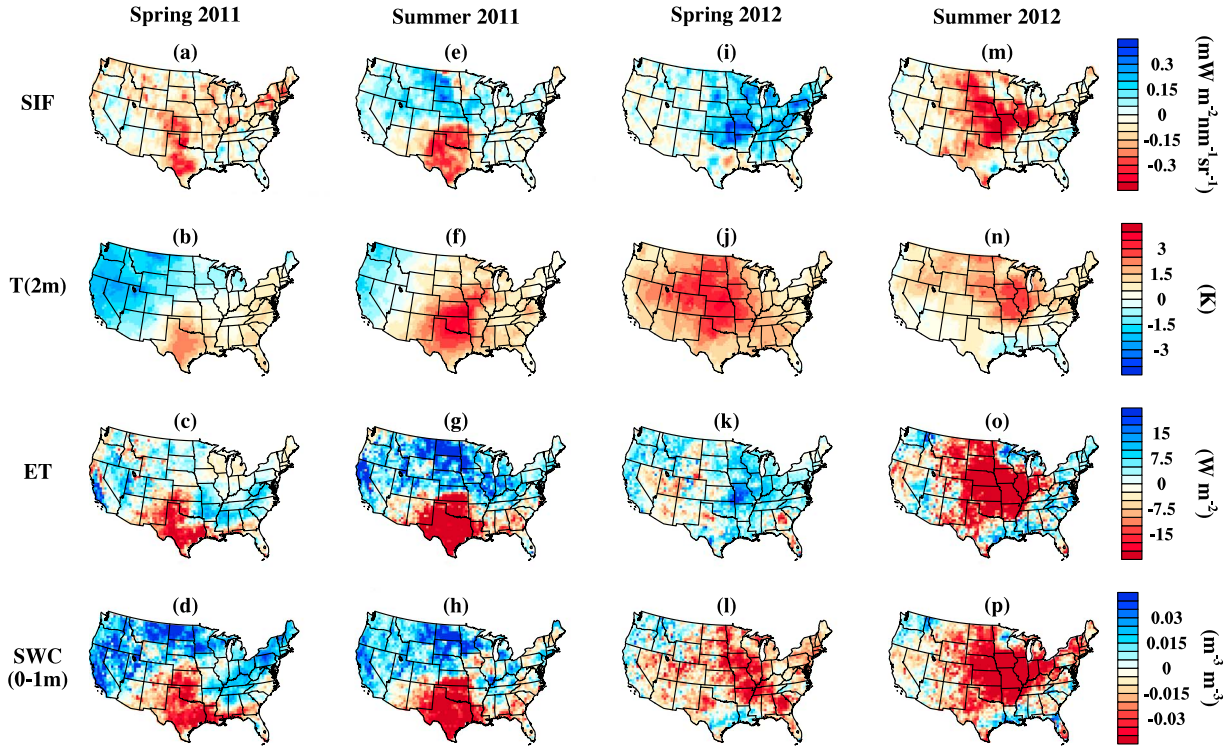

Figure 3. The spatial distributions of the anomalies of SIF, T2m, ET, and root zone SWC for the U.S. during (a–h) the 2011 Texas drought and (i–p) the 2012 central Great Plains drought. Spring (April and May) and summer (June, July, and August) anomalies are separated, demonstrating the dynamic development of two drought events.

rapidly than the multiyear mean (Figure 2f), as also did ET (Figure 2h). This rise was apparently caused by favorable conditions for vegetation growth in early 2012. The temperature was warmer (Figure 2g) and the precipitation was similar to multiyear mean (Figure 2j), while the soil moisture was only slightly below normal (Figure 2i). However, by May, the vegetation growth conditions in the Great Plains started to deteriorate as the precipitation turned from above to below normal and the soil moisture deficit widened sharply. The persistently high spring temperatures, among other factors, probably exacerbated the sharp decline of soil moisture in summer. This deteriorating growth condition led to the change of the monthly GOME-2 SIF around May from being higher than normal to less than normal. Its departure from normal widened until some precipitation events occurred and resupplied moisture to the soil late in the summer. Similar to the 2011 Texas drought, the simulated ET showed temporal dynamics broadly resembling that of the GOME-2 SIF with some difference occurring around the time when the drought started to break (Figure 2h). As in the 2011 Texas event, the spatial distributions of the SIF anomalies and environmental variables revealed the dynamic progression of drought from spring to summer of 2012 in the central Great Plains (Figures 3i–3p).

The PAR-normalized SIF (i.e., equations (2) and (3)) provides further insights into the component processes that were responsible for the drought-induced changes in SIF during the two droughts (Figure 4). Once the effects of seasonal variations in PAR were removed (equation (2)), the drought impacts on SIF became more pronounced for both drought events and the contrast between them became clearer (compare Figures 2a and 2f with Figures 4a and 4d, respectively). Sustained decrease in fPAR (Figure 4b) and in the effective fluorescence yield (equation (3) and Figure 4c) was observed in 2011 for the Texas drought. For the 2012 event in the central Great Plains, both fPAR (Figure 4e) and the effective fluorescence yield (Figure 4f) were higher than the corresponding multiyear mean for early spring but this pattern was reversed in the rest of the year. Thus, our results indicate that both fPAR and the effective fluorescence yield were affected by the droughts and contributed to the observed dynamics of SIF.

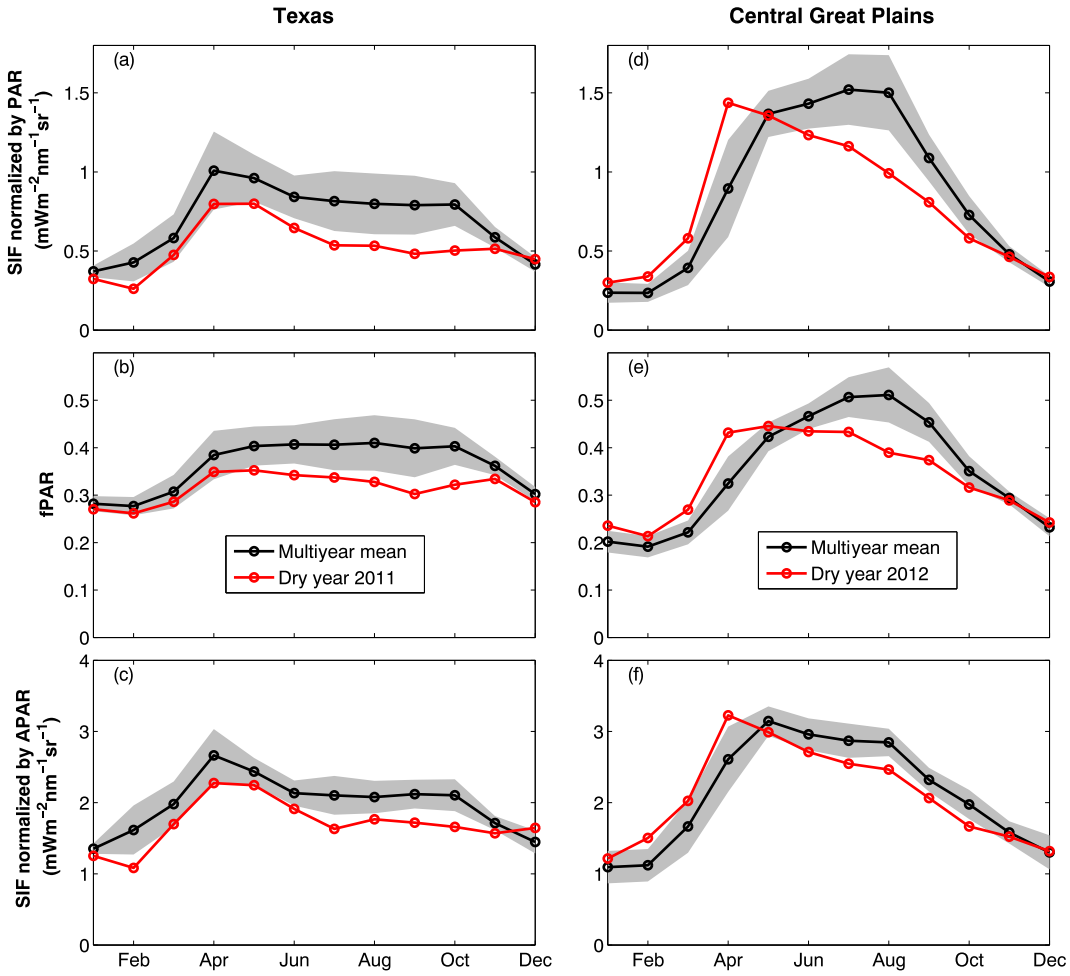

Figure 4. The region-wide mean seasonal cycle of (a and d) SIF normalized by photosynthetically active radiation (PAR) (i.e., divided by cosine of solar zenith angle cos (Z), (b and e) fraction of absorbed PAR (fPAR), and (c and f) SIF normalized by the absorbed PAR (APAR) (i.e., PAR-normalized SIF further divided by fPAR), which is related to fluorescence yield.

The seasonal pattern of the PAR-normalized multiyear mean SIF is dominated by that of fPAR in the central Great Plains (compare Figures 4d and 4e). However, during 2012, the pattern was more similar to that of the effective fluorescence yield than to that of fPAR (compare Figures 4d and 4f). In particular, both the PAR-normalized SIF and the effective fluorescence yield peaked in April 2012 and then declined steadily afterward. In contrast, fPAR was relatively stable from April to July 2012. This indicates that the steady decrease in the effective fluorescence yield was responsible for the decreasing trend in the PAR-normalized SIF from its early spring peak in 2012. Only after July 2012, fPAR started to decline and its significant deviation from the multiyear mean contributed to the SIF reduction. For Texas, the seasonal pattern of the PAR-normalized SIF (Figure 4a) was more similar to that of the effective fluorescence yield (Figure 4c) than to that of fPAR for both the 2011 drought and the multiyear mean.

Therefore, our analyses indicate that the GOME-2 SIF not only depicts the spatial extension of both drought events but also captures the temporal dynamics of their impacts on fPAR and effective fluorescence yield. These qualitative analyses are corroborated by the quantification of the relationships of SIF with key drought sensitive variables in a broader context in Figure 5. Both in Texas (Figure 5a) and in the central Great Plains (Figure 5b), the anomalies of GOME-2 SIF are significantly positively correlated with the anomalies of root zone SWC across June, July, and August. The SIF-SWC correlations tend to be stronger in summer than in spring and fall especially in the central Great Plains (Figures 5c and 5d). In addition to SWC, the SIF anomalies also show significant positive correlation with ET (Figures 5c and 5d). In contrast, the correlation of SIF and

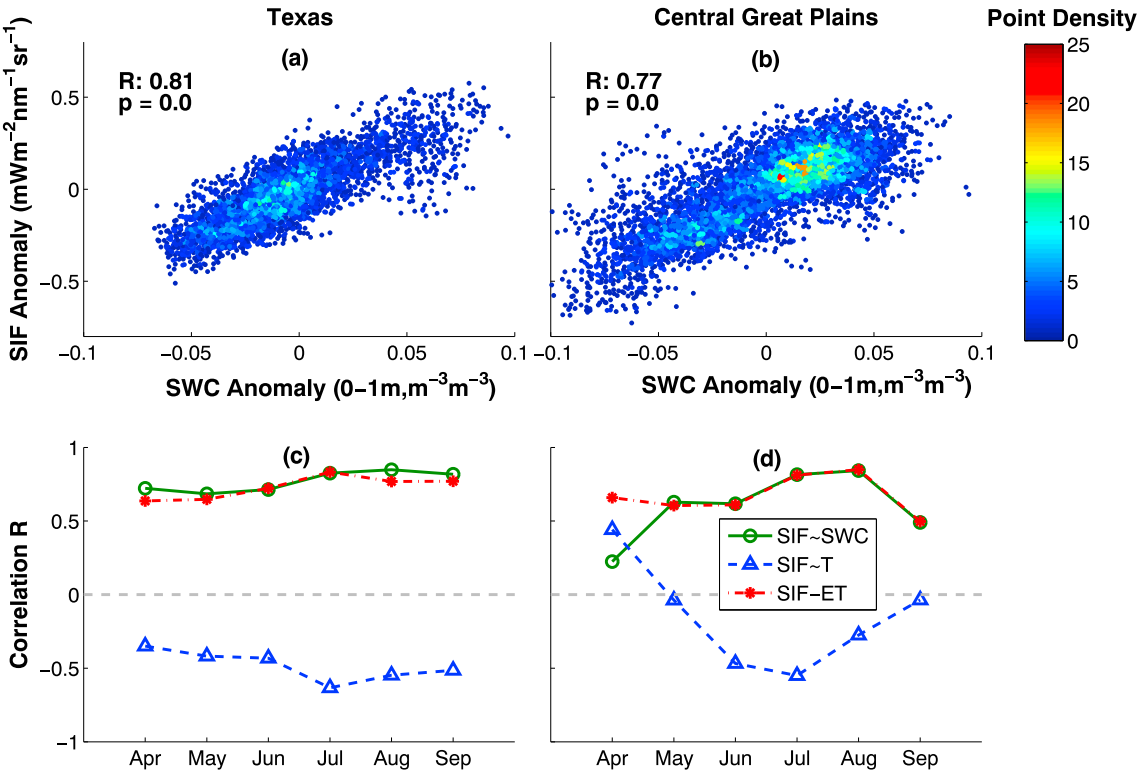

Figure 5. Relationships between (a, b) the summertime root zone SWC anomaly and SIF anomaly (left: Texas; right: central Great Plains). Each dot represents a grid cell within the defined areas in Figure 1 in a month from June to August between 2007 and 2013. Color demonstrates the density of dot distribution. The correlation coefficients (*R*) and associated *p* values are also shown. (c, d) Monthly temporal evolution of the correlation of all grid cells in each month among anomalies of SIF with SWC, ET, and temperature.

temperature anomalies is more complicated. In Texas where climate is relatively warm, the SIF-*T* correlation is negative throughout the growing season. In the central Great Plains, the correlation was only negative in the summer but positive in spring, because of temperature control on spring phenology rather than soil moisture in this region. The strong correlations of GOME-2 SIF with SWC, temperature, and ET are also reflected in the striking resemblance between the spatial distributions of the anomalies of these variables for the spring and summer of 2011 and 2012 (Figure 3).

4. Discussion and Conclusion

This study indicates that satellite-based SIF reasonably characterizes the spatial and temporal dynamics of drought development and identifies regions with varying drought severity. Severe summer drought onset can either follow a strong soil moisture deficit in spring due to lack of rainfall, such as during the 2011 Texas drought [*Fernando et al*., 2015] or a relatively normal rainfall and warm spring but a sudden rainfall deficit in summer, such as during the 2012 central Great Plains drought [*Hoerling et al*., 2014]. Such differences in drought onset mechanisms lead to different soil moisture regimes, which in turn have contrasting impacts on the development of plant activity. For the first type of drought, soil moisture constrained vegetation growth in both spring and summer. For the second, "flash" type of drought, vigorous photosynthetic activity in spring was stimulated by favorable temperatures, exhausting soil water supply, and amplifying the sharp drop of soil water storage caused by sudden precipitation depletion later in the summer. The SIF signal can well capture such contrasting dynamics of vegetation functioning and thus provide insights for interpreting the development of drought.

In summertime, large decreases in the GOME-2 SIF occurred for both the Texas and central Great Plains droughts. This happened because water supply is the limiting factor that determines plant photosynthesis in summer, allowing the soil moisture deficit to be well tracked by abnormally low SIF values. The strong

SIF-SWC relationship revealed in this study indicates a potential of using SIF as a proxy for root zone soil moisture for characterizing agricultural drought.

The SIF-soil moisture-drought relationship depends on variations of both APAR (or fPAR) and fluorescence yield in response to water stress. Under extreme drought, for example, the two events examined in our study, photosynthetic pigments can degrade and LAI decrease. Severe drought stress can also cause leaf wilting, a sign of plant turgor loss or can trigger leaf movement and rolling, all of which can reduce effective LAI. All these potential foliar changes reduce fPAR and therefore the energy for both photosynthesis and fluorescence emission [*Porcar-Castell et al*., 2014]. Presumably, some combination of these changes occurred for both of our events as we observed the simultaneous drought responses of fPAR and SIF. In particular, when drought starts before and persists throughout the growing season, plant phenology of the whole growing season may be adapted to a new drought regime with sustained reduction in LAI, leading to a season-wide suppression of photosynthesis and SIF.

Variations in SIF caused by changes in fluorescence yield are more complex. Our results indicate that both drought events depressed the effective fluorescence yield of the vegetation in the study regions. Changes in fluorescence yield may occur without concurrent changes in chlorophyll content and phenology, as for example, in cases of relatively mild stress conditions compared to that of an extreme drought. Water deficit usually induces stomatal closure and hence reduction of CO_2 uptake, which in turn slows down photosynthesis. This reduces the proportion of APAR that is used to drive electron transport for carbon assimilation, or "photochemical yield," but this does not necessarily mean more APAR is available for fluorescing as the heat dissipation via NPQ may increase to a level that compensates for the effect of reduced photochemical yield, leading to a decrease of fluorescence yield and hence SIF (if there are no concurrent changes of chlorophyll content or LAI) [*Flexas et al*., 2002; *Daumard et al*., 2010]. Although both SIF and fPAR are responsive to chlorophyll content and LAI, SIF but not fPAR is sensitive to variations in fluorescence yield.

In a broad context, the sensitivity of satellite-observed SIF to the environmental variables that influence vegetation growth is complicated, because fluorescence yield is affected by biotic (species types, photosynthetic capacities, etc.) and abiotic factors (e.g., nutrient availability, temperature, CO_2 concentration, and radiation) in complex nonlinear ways [*Porcar-Castell et al*., 2014]. Our inference of the drought effects on fluorescence yield is indirect as it relies on the remote sensing of fPAR as an input, which may also contain errors. The fPAR product used here is affected by not just green leaves but also by nongreen elements such as branches, stems, and soils, which could confound the inference of the effective fluorescence yield. Also, it is possible that the relatively simple linear correlative analyses in this study (e.g., Figure 5) may have primarily captured stress-induced changes in chlorophyll content and LAI but not sufficiently in fluorescence yield. Additional analyses could be performed with models that explicitly represent SIF processes [e.g., *van der Tol et al*., 2014; *Lee et al*., 2015], so that one can further attribute the stress-induced variations of SIF to different sources. For example, *Yoshida et al*. [2015] have used model-simulated SIF to examine the 2010 Russian drought and found that it is broadly consistent with satellite-observed SIF pattern. This work further partitioned the SIF variations (for both satellite and modeled data sets) into fluorescence yield and fPAR, similar to our analysis. Nevertheless, more process-based studies of responses of leaf-, canopy-, and landscape-scale fluorescence to environmental stresses with better temporally resolved experiments are needed. With guidance and data from such studies, more sophisticated analyses of responses of SIF from satellite remote sensing to environmental stresses can be developed.

Future satellite SIF products would be improved by tracking SIF variation on a subdaily scale. Field studies have shown that the sensitivity of fluorescence yield to water stress is higher in the afternoon when plants water stress tends to peak [*Daumard et al*., 2014]. The current GOME-2 SIF is measured at a local overpass time of 09:30 A.M., when physiological water stress tends to be diminished by the resupply of plant water overnight and by the relatively low atmospheric vapor pressure deficit in the early morning. Future satellite fluorescence missions would be improved by measurement of SIF both in the morning and afternoon. At present, such morning-afternoon observation coupling may be obtained by combining data sets from GOME-2 with those of the Orbiting Carbon Observatory-2 (OCO-2) [*Frankenberg et al*., 2014] or could be explored after the future launch of TROPOspheric Monitoring Instrument [*Guanter et al*., 2015]. Thus, with improved spatial resolution, timing of observation, sampling density, and retrieval methods coupled with better mechanistic understanding of solar energy partitioning at the leaf scale, future satellite SIF products should better serve drought monitoring needs.

The Texas region appears to have a tighter coupling in summer months between SIF and the modeled soil moisture than the central Great Plains (compare Figures 5a with 5b). This regional difference may be caused by a lack of representing irrigation in NLDAS-2 models [*Xia et al*., 2014b], a process that is critical for plant and crop growth in the central Great Plains. In addition, the simulated soil moisture can also be biased by factors such as uncertainties in atmospheric forcing, model parameters of soil properties, model structural deficiencies, etc. But overall, NLDAS-2 land surface models are able to simulate soil moisture that can reasonably track the wet/dry variations compared to measurements [*Xia et al*., 2014b] and so capture the considerable drawdown of soil moisture in extreme drought events as shown in this study. The close relationship between simulated soil moisture and satellite SIF confirms the usefulness of these model products in large-scale drought monitoring.

In summary, we find that satellite-based SIF has potential for characterizing and monitoring the spatial and temporal dynamics of drought in vegetated regions. Using the droughts of 2011 in Texas and 2012 in the central Great Plains as two case studies, we found that the satellite SIF anomalies can be used as a measure of drought intensity in general and root zone soil moisture deficit in particular. The significant correlations of SIF with drought-induced anomalies in key environmental variables and their spatial and temporal variations are consistent with the expectation that SIF measures the physiological and biochemical state of vegetation and is a direct signal of vegetation photosynthetic functioning. Future applications of satellite SIF could be improved by better timing of observations, higher spatial resolution, and modeling of processes controlling energy partitioning within the photosynthetic machinery.

Acknowledgments

We thank John Michael Wallace, Kingtse Mo, Ranga Myneni, and Kevin Bowman for helpful discussions, Yasuko Yoshida for providing SIF model products and Xitian Cai for clarification of NLDAS-2 soil moisture datasets. The support for this research came from NASA the Development and Testing of Potential Indicators for the National Climate Assessment Program (grant NNX13AN39G awarded to The University of Texas at Austin). L.Gu was supported by the U.S. Department of Energy, Office of Science, Office of Biological and Environmental Research Program, Climate and Environmental Sciences Division. ORNL is managed by UT-Battelle, LLC, for the U.S. Department of Energy under contract DE-AC05-00OR22725. The GOME-2 v26 level 3 SIF data are publicly available at http://avdc.gsfc.nasa.gov. The GOSAT SIF product is available in *Frankenberg et al*. [2011b]. The NLDAS-2 products and MODIS fPAR are obtained from http://ldas.gsfc.nasa.gov/nldas/ and https://lpdaac.usgs.gov/, respectively.

References

Baker, N. R. (2008), Chlorophyll fluorescence: A probe of photosynthesis in vivo, *Annu. Rev. Plant Biol.*, *59*, 89–113.

Ball, J. T., I. E. Woodrow, and J. A. Berry (1987), A model predicting stomatal conductance and its contribution to the control of photosynthesis under different environmental conditions, in *Progress in Photosynthesis Research*, vol. 4, edited by J. Biggens, pp. 221–224, Martinus Nijhoff Publishers, Dordrecht, Netherlands.

Brown, J. F., B. D. Wardlow, T. Tadesse, M. J. Hayes, and B. C. Reed (2008), The Vegetation Drought Response Index (VegDRI): A new integrated approach for monitoring drought stress in vegetation, *GIScience Remote Sens.*, *45*(1), 16–46, doi:10.2747/1548-1603.45.1.16.

Combs, S. (2012), The impact of Texas' 2011 drought and beyond, Texas Comptroller of Public Accounts Spec. Rep., Publ. 96-1704, 16 pp.

Cook, B. I., T. R. Ault, and J. E. Smerdon (2015), Unprecedented 21st century drought risk in the American Southwest and Central Plains, *Sci. Adv.*, *1*(1), e1400082, doi:10.1126/sciadv.1400082.

Cook, E. R., R. Seager, M. A. Cane, and D. W. Stahle (2007), North American drought: Reconstructions, causes, and consequences, *Earth Sci. Rev.*, *81*(1–2), 93–134, doi:10.1016/j.earscirev.2006.12.002.

Damm, A., L. Guanter, E. Paul-Limoges, C. van der Tol, A. Hueni, N. Buchmann, W. Eugster, C. Ammann, and M. E. Schaepman (2015), Far-red sun-induced chlorophyll fluorescence shows ecosystem-specific relationships to gross primary production: An assessment based on observational and modeling approaches, *Remote Sens. Environ.*, *166*, 91–105, doi:10.1016/j.rse.2015.06.004.

Daumard, F., S. Champagne, A. Fournier, Y. Goulas, A. Ounis, J.-F. Hanocq, and I. Moya (2010), A field platform for continuous measurement of canopy fluorescence, *IEEE Trans. Geosci. Remote Sens.*, *48*(9), 3358–3368, doi:10.1109/TGRS.2010.2046420.

Daumard, F., I. Moya, Y. Goulas, A. Ounis, and C. Rhoul (2014), GFLEX: Monitoring the diurnal time course of vegetation dynamics with geostationary. [Available at http://congrexprojects.com/Custom/14C04/Papers/Oral%20Presentations/S2_1710_Daumard.pdf.]

Ek, M. B., K. E. Mitchell, Y. Lin, E. Rogers, P. Grunmann, V. Koren, G. Gayno, and J. D. Tarpley (2003), Implementation of Noah land surface model advances in the National Centers for Environmental Prediction operational mesoscale Eta model, *J. Geophys. Res.*, *108*(D22), 8851, doi:10.1029/2002JD003296.

Fannin, B. (2012), Updated 2011 Texas agricultural drought losses total $7.62 billion, AgriLife Today.

Fernando, N. D., R. Fu, R. S. Solis, R. E. Mace, Y. Sun, B. Yan, and B. Pu (2015), Early warning of summer drought over Texas and the south central United States: Spring conditions as a harbinger of summer drought, Austin. [Available at http://www.twdb.texas.gov/newsmedia/press_releases/2015/02/drought.asp.]

Flexas, J., J. M. Escalona, S. Evain, J. Gulias, I. Moya, C. B. Osmond, and H. Medrano (2002), Steady-state chlorophyll fluorescence (Fs) measurements as a tool to follow variations of net CO_2 assimilation and stomatal conductance during water-stress in C3 plants, *Physiol. Plant.*, *114*(2), 231–240, doi:10.1034/j.1399-3054.2002.1140209.x.

Frankenberg, C., A. Butz, and G. C. Toon (2011a), Disentangling chlorophyll fluorescence from atmospheric scattering effects in O 2 A-band spectra of reflected sun-light, *Geophys. Res. Lett.*, *38*, L03801, doi:10.1029/2010GL045896.

Frankenberg, C., et al. (2011b), New global observations of the terrestrial carbon cycle from GOSAT: Patterns of plant fluorescence with gross primary productivity, *Geophys. Res. Lett.*, *38*, L17706, doi:10.1029/2011GL048738.

Frankenberg, C., C. O'Dell, J. Berry, L. Guanter, J. Joiner, P. Köhler, R. Pollock, and T. E. Taylor (2014), Prospects for chlorophyll fluorescence remote sensing from the Orbiting Carbon Observatory-2, *Remote Sens. Environ.*, *147*, 1–12, doi:10.1016/j.rse.2014.02.007.

Gilbert, N. (2012), Drought devastates US crops, *Nature*, doi:10.1038/nature.2012.11065.

Guanter, L., L. Alonso, L. Gómez-Chova, J. Amorós-López, J. Vila, and J. Moreno (2007), Estimation of solar-induced vegetation fluorescence from space measurements, *Geophys. Res. Lett.*, *34*, L08401, doi:10.1029/2007GL029289.

Guanter, L., C. Frankenberg, A. Dudhia, P. E. Lewis, J. Gómez-Dans, A. Kuze, H. Suto, and R. G. Grainger (2012), Retrieval and global assessment of terrestrial chlorophyll fluorescence from GOSAT space measurements, *Remote Sens. Environ.*, *121*, 236–251, doi:10.1016/j.rse.2012.02.006.

Guanter, L., et al. (2014), Global and time-resolved monitoring of crop photosynthesis with chlorophyll fluorescence, *Proc. Natl. Acad. Sci. U.S.A.*, *111*(14), E1327–33, doi:10.1073/pnas.1320008111.

Guanter, L., I. Aben, P. Tol, J. M. Krijger, A. Hollstein, P. Köhler, A. Damm, J. Joiner, C. Frankenberg, and J. Landgraf (2015), Potential of the TROPOspheric Monitoring Instrument (TROPOMI) onboard the Sentinel-5 precursor for the monitoring of terrestrial chlorophyll fluorescence, *Atmos. Meas. Tech.*, *8*(3), 1337–1352, doi:10.5194/amt-8-1337-2015.

Hoerling, M., J. Eischeid, A. Kumar, R. Leung, A. Mariotti, K. Mo, S. Schubert, and R. Seager (2014), Causes and predictability of the 2012 great plains drought, *Bull. Am. Meteorol. Soc.*, *95*(2), 269–282, doi:10.1175/BAMS-D-13-00055.1.

Hoerling, M. P., J. K. Eischeid, X.-W. Quan, H. F. Diaz, R. S. Webb, R. M. Dole, and D. R. Easterling (2012), Is a transition to semipermanent drought conditions imminent in the U.S. Great Plains?, *J. Clim.*, *25*(24), 8380–8386, doi:10.1175/JCLI-D-12-00449.1.

Hsiao, T. C. (1973), Plant responses to water stress, *Annu. Rev. Plant Physiol.*, *24*, 519–570.

Huete, A., K. Didan, T. Miura, E. P. Rodriguez, X. Gao, and L. G. Ferreira (2002), Overview of the radiometric and biophysical performance of the MODIS vegetation indices, *Remote Sens. Environ.*, *83*(1–2), 195–213, doi:10.1016/S0034-4257(02)00096-2.

Joiner, J., Y. Yoshida, A. P. Vasilkov, L. A. Corp, and E. M. Middleton (2011), First observations of global and seasonal terrestrial chlorophyll fluorescence from space, *Biogeosciences*, *8*(3), 637–651, doi:10.5194/bg-8-637-2011.

Joiner, J., Y. Yoshida, A. P. Vasilkov, E. M. Middleton, P. K. E. Campbell, Y. Yoshida, A. Kuze, and L. A. Corp (2012), Filling-in of near-infrared solar lines by terrestrial fluorescence and other geophysical effects: Simulations and space-based observations from SCIAMACHY and GOSAT, *Atmos. Meas. Tech.*, *5*, 809–829, doi:10.5194/amt-5-809-2012.

Joiner, J., L. Guanter, R. Lindstrot, M. Voigt, A. P. Vasilkov, E. M. Middleton, K. F. Huemmrich, Y. Yoshida, and C. Frankenberg (2013), Global monitoring of terrestrial chlorophyll fluorescence from moderate-spectral-resolution near-infrared satellite measurements: Methodology, simulations, and application to GOME-2, *Atmos. Meas. Tech.*, *6*(10), 2803–2823, doi:10.5194/amt-6-2803-2013.

Joiner, J., et al. (2014), The seasonal cycle of satellite chlorophyll fluorescence observations and its relationship to vegetation phenology and ecosystem atmosphere carbon exchange, *Remote Sens. Environ.*, *152*, 375–391, doi:10.1016/j.rse.2014.06.022.

Kogan, F. N. (1995), Application of vegetation index and brightness temperature for drought detection, *Adv. Space Res.*, *15*(11), 91–100, doi:10.1016/0273-1177(95)00079-T.

Koster, R. D., and M. J. Suarez (1992), Modeling the land surface boundary in climate models as a composite of independent vegetation stands, *J. Geophys. Res.*, *97*(D3), 2697, doi:10.1029/91JD01696.

Lee, J.-E., et al. (2013), Forest productivity and water stress in Amazonia: Observations from GOSAT chlorophyll fluorescence, *Proc. Biol. Sci.*, *280*(1761), 20130171, doi:10.1098/rspb.2013.0171.

Lee, J.-E., J. A. Berry, C. van der Tol, X. Yang, L. Guanter, A. Damm, I. Baker, and C. Frankenberg (2015), Simulations of chlorophyll fluorescence incorporated into the Community Land Model version 4, *Global Change Biol.*, doi:10.1111/gcb.12948.

Liang, X., D. P. Lettenmaier, E. F. Wood, and S. J. Burges (1994), A simple hydrologically based model of land surface water and energy fluxes for general circulation models, *J. Geophys. Res.*, *99*(D7), 14,415–14,428, doi:10.1029/94JD00483.

Liu, W. T., and F. N. Kogan (1996), Monitoring regional drought using the Vegetation Condition Index, *Int. J. Remote Sens.*, *17*(14), 2761–2782.

Long, D., B. R. Scanlon, L. Longuevergne, A. Y. Sun, D. N. Fernando, and H. Save (2013), GRACE satellite monitoring of large depletion in water storage in response to the 2011 drought in Texas, *Geophys. Res. Lett.*, *40*, 3395–3401, doi:10.1002/grl.50655.

Long, D., L. Longuevergne, and B. R. Scanlon (2014), Uncertainty in evapotranspiration from land surface modeling, remote sensing, and GRACE satellites, *Water Resour. Res.*, *50*, 1131–1151, doi:10.1002/2013WR014581.

Mesinger, F., et al. (2006), North American regional reanalysis, *Bull. Am. Meteorol. Soc.*, *87*, 343–360, doi:10.1175/BAMS-87-3-343.

Mo, K. C., and D. P. Letternmaier (2015), Heat wave flash droughts in decline, *Geophys. Res. Lett.*, *42*, 2823–2829, doi:10.1002/2015GL064018.

Mu, Q., M. Zhao, J. S. Kimball, N. G. McDowell, and S. W. Running (2013), A remotely sensed global terrestrial drought severity index, *Bull. Am. Meteorol. Soc.*, *94*(1), 83–98, doi:10.1175/BAMS-D-11-00213.1.

Myneni, R. B., et al. (2002), Global products of vegetation leaf area and fraction absorbed PAR from year one of MODIS data, *Remote Sens. Environ.*, *83*, 214–231.

Porcar-Castell, A., E. Tyystjärvi, J. Atherton, C. Van Der Tol, J. Flexas, E. E. Pfündel, J. Moreno, C. Frankenberg, and J. A. Berry (2014), Linking chlorophyll a fluorescence to photosynthesis for remote sensing applications: Mechanisms and challenges, *J. Exp. Bot.*, *65*(15), 4065–4095.

Seager, R., L. Goddard, J. Nakamura, N. Henderson, and D. E. Lee (2014), Dynamical causes of the 2010/11 Texas–Northern Mexico Drought*, *J. Hydrometeorol.*, *15*(1), 39–68, doi:10.1175/JHM-D-13-024.1.

Sheffield, J., Y. Xia, L. Luo, E. F. Wood, M. Ek, and K. E. Mitchell (2012), North American land data assimilation system, in *Remote Sensing of Drought: Innovative Monitoring Approaches*, edited by B. D. Wardlow, M. C. Anderson, and J. P. Verdin, pp. 227–260, CPC Press, Boca Raton.

Smith, A. B., and J. L. Matthews (2015), Quantifying uncertainty and variable sensitivity within the US billion-dollar weather and climate disaster cost estimates, *Nat. Hazards*, doi:10.1007/s11069-015-1678-x.

Svoboda, M., et al. (2002), The drought monitor, *Bull. Am. Meteorol. Soc.*, *83*(8), 1181–1190.

van der Tol, C., W. Verhoef, A. Timmermans, A. Verhoef, and Z. Su (2009), An integrated model of soil-canopy spectral radiances, photosynthesis, fluorescence, temperature and energy balance, *Biogeosciences*, *6*, 3109–3129.

van der Tol, C., J. A. Berry, P. K. E. Campbell, and U. Rascher (2014), Models of fluorescence and photosynthesis for interpreting measurements of solar-induced chlorophyll fluorescence, *J. Geophys. Res. Biogeosci.*, *119*, 2312–2327, doi:10.1002/2014JG002713.

Wardlow, B. D., T. Tadesse, J. F. Brown, K. Callahan, S. Swain, and E. Hunt (2012), Vegetation drought response index: An integration of satellite, climate, and biophysical data, in *Remote Sensing of Drought: Innovative Monitoring Approaches*, edited by B. D. Wardlow, M. C. Anderson, and J. P. Verdin, pp. 51–74, CPC Press, Boca Raton, Fla.

Xia, Y., et al. (2012), Continental-scale water and energy flux analysis and validation for the North American Land Data Assimilation System project phase 2 (NLDAS-2): 1. Intercomparison and application of model products, *J. Geophys. Res.*, *117*, D03109, doi:10.1029/2011JD016048.

Xia, Y., M. B. Ek, C. D. Peters-Lidard, D. Mocko, M. Svoboda, J. Sheffield, and E. F. Wood (2014a), Application of USDM statistics in NLDAS-2: Optimal blended NLDAS drought index over the continental United States, *J. Geophys. Res. Atmos.*, *119*, 2947–2965, doi:10.1002/2013JD020994.

Xia, Y., J. Sheffield, M. B. Ek, J. Dong, N. Chaney, H. Wei, J. Meng, and E. F. Wood (2014b), Evaluation of multi-model simulated soil moisture in NLDAS-2, *J. Hydrol.*, *512*, 107–125, doi:10.1016/j.jhydrol.2014.02.027.

Xia, Y., M. T. Hobbins, Q. Mu, and M. B. Ek (2015), Evaluation of NLDAS-2 evapotranspiration against tower flux site observations, *Hydrol. Processes*, *29*(7), 1757–1771, doi:10.1002/hyp.10299.

Xu, L., A. Samanta, M. H. Costa, S. Ganguly, R. R. Nemani, and R. B. Myneni (2011), Widespread decline in greenness of Amazonian vegetation due to the 2010 drought, *Geophys. Res. Lett.*, *38*, L07402, doi:10.1029/2011GL046824.

Yang, X., J. Tang, J. F. Mustard, J.-E. Lee, M. Rossini, J. Joiner, J. W. Munger, A. Kornfeld, and A. D. Richardson (2015), Solar-induced chlorophyll fluorescence that correlates with canopy photosynthesis on diurnal and seasonal scales in a temperate deciduous forest, *Geophys. Res. Lett.*, *42*, 2977–2987, doi:10.1002/2015GL063201.

Yoshida, Y., J. Joiner, C. Tucker, J. Berry, J.-E. Lee, G. Walker, R. Reichle, R. Koster, A. Lyapustin, and Y. Wang (2015), The 2010 Russian drought impact on satellite measurements of solar-induced chlorophyll fluorescence: Insights from modeling and comparisons with parameters derived from satellite reflectances, *Remote Sens. Environ.*, *166*, 163–177, doi:10.1016/j.rse.2015.06.008.

Zhou, L., et al. (2014), Widespread decline of Congo rainforest greenness in the past decade, *Nature*, *509*(7498), 86–90.